Materials Science & Engineering C 107 (2020) 110301

Contents lists available at ScienceDirect

Materials Science & Engineering C

journal homepage: www.elsevier.com/locate/msec

Improved vascularisation but inefficient *in vivo* bone regeneration of adipose stem cells and poly-3-hydroxybutyrate-co-3-hydroxyvalerate scaffolds in xeno-free conditions

Ana C.C. Paula[a,b,*], Pablo H. Carvalho[c], Thaís M.M. Martins[d], Jankerle N. Boeloni[e], Pricila S. Cunha[a], Silviene Novikoff[a,j], Vitor M. Correlo[f,g,h], Rui L. Reis[f,g,h], Alfredo M. Goes[a,i]

[a] Department of Biochemistry and Immunology, Institute of Biological Sciences, Federal University of Minas Gerais, Av. Presidente Antônio Carlos, 6627, Belo Horizonte, 31270-901, MG, Brazil
[b] Department of Pharmaceutical Sciences, School of Pharmacy, Federal University of Juiz de Fora, R. José Lourenço Kelmer- s/n, Juiz de Fora, 36036-900, MG, Brazil
[c] Department of Clinical and Surgery, College of Veterinary Medicine, Federal University of Minas Gerais, Av. Presidente Antônio Carlos- 6627, Belo Horizonte, 31270-901, MG, Brazil
[d] Department of Morphology, Institute of Biological Sciences, Federal University of Minas Gerais, Av. Presidente Antônio Carlos- 6627, Belo Horizonte, 31270-901, MG, Brazil
[e] Department of Veterinary Medicine, Federal University of Espírito Santo, Alto Universitário, Alegre, 29500-000, ES, Brazil
[f] 3B´s Research Group, I3Bs - Research Institute on Biomaterials, Biodegradables and Biomimetics, University of Minho, Headquarters of the European Institute of Excellence on Tissue Engineering and Regenerative Medicine, AvePark, Parque de Ciência e Tecnologia, Zona Industrial de Gandra, 4805-017, Barco, Guimarães, Portugal
[g] ICVS/3B's - Associate Laboratory, PT Government Associate Laboratory, Campus de Gualtar, 4710-057, Braga, Portugal
[h] The Discoveries Centre for Regenerative and Precision Medicine, Headquarters at University of Minho, Avepark, 4805-017, Barco, Guimarães, Portugal
[i] Department of Pathology, Institute of Biological Sciences, Federal University of Minas Gerais, Av. Presidente Antônio Carlos- 6627, Belo Horizonte, 31270-901, MG, Brazil
[j] Transplants Immunobiology Laboratory, Department of Immunology, University of São Paulo, Brazil

ARTICLE INFO

Keywords:
Tissue engineering
Adipose stem cells
PHB-HV
Neovascularisation
Bone

ABSTRACT

Bone defects are a common clinical situation. However, bone regeneration remains a challenge and faces the limitation of poor engraftment due to deficient vascularisation. Poly-3-hydroxybutyrate-co-3-hydroxyvalerate (PHB-HV) and human adipose stem cells (hASC) are promising for vascularisation and bone regeneration. Therefore, we sought to investigate the bone regenerative capacity of hASCs cultured in allogeneic human serum (aHS) and PHB-HV scaffolds in a nude mouse model of the critical-sized calvarial defect. We evaluated bone healing for three treatment groups: empty (control), PHB-HV and PHB-HV + hASCs. The pre-implant analysis showed that hASCs colonised the PHB-HV scaffolds maintaining cell viability before implantation. Histological analysis revealed that PHB-HV scaffolds were tolerated *in vivo*; they integrated with adjacent tissue eliciting a response like a foreign body reaction, and tiny primary bone was observed only in the PHB-HV group. Also, the μ-CT analysis revealed only approximately 10% of new bone in the bone defect area in both the PHB-HV and PHB-HV + hASCs groups. The expression of *BGLAP* and its protein (osteocalcin) by PHB-HV + hASCs group and native bone was similar while the other bone markers *RUNX2*, *ALPL* and *COL1A1* were upregulated, but this expression remained significantly lower compared to the native bone. Nevertheless, the PHB-HV group showed neovascularisation at 12 weeks post-implantation while PHB-HV + hASCs group also exhibited higher *VEGFA* expression as well as a higher number of vessels at 4 weeks post-implantation, and, consequently, earlier neovascularisation. This neovascularisation must be due to scaffold architecture, improved by hASCs, that survived for the long term *in vivo* in the PHB-HV + hASCs group. These results demonstrated that hASCs cultured in aHS combined with PHB-HV scaffolds were ineffective to promote bone regeneration, although the construct of hASCs + PHB-HV in xeno-free conditions improved scaffold vascularisation representing a strategy potentially promising for other tissue engineering applications.

Abbreviations: hASCs, human adipose stem cells; aHS, allogeneic human serum; PHB-HV, poly-3-hydroxybutyrate-co-3-hydroxyvalerate; FBS, fetal bovine serum; PHB, poly-3-hydroxybutyrate; PHA, polyhydroxyalkanoates; HAP, hydroxyapatite

* Corresponding author. Department of Pharmaceutical Sciences, School of Pharmacy, Federal University of Juiz de Fora, R. José Lourenço Kelmer - s/n, Juiz de Fora, 36036-900, Brazil.
E-mail address: anachagas.paula@ufjf.edu.br (A.C.C. Paula).

https://doi.org/10.1016/j.msec.2019.110301
Received 28 August 2019; Received in revised form 24 September 2019; Accepted 10 October 2019
Available online 12 October 2019
0928-4931/

1. Introduction

Regeneration of bone defects that arise from trauma, congenital defects, infections and tumour excision remains a clinical challenge [1]. Autologous bone grafting is the standard gold treatment for non-healing, critical-sized bone defects since the grafts would be histocompatible and non-immunogenic; however, this procedure has significant drawbacks, such as a second surgery site, discomfort, pain and donor site morbidity. Allografting also has several disadvantages that limit its use, including reduced bioactivity and increased risk of disease transmission [1,2]. Furthermore, the quantity of tissue that can be harvested without the morbidity of the donor site is limited. Despite commercially-available bone products for orthopaedic treatment, regeneration of critical-sized bone defects remains elusive [3]. In this scenario, tissue engineering has shown therapeutic advantages by delivering cells and growth factors in biodegradable scaffolds. These structures supply the necessary cues to recreate a suitable niche for the restoration, maintenance and improvement of tissue function [4].

In this way, various biomaterials, such polymers (e.g., poly-3-hydroxybutyrate (PHB), poly L-lactic acid (PLLA), polycaprolactone, poly (glycolic acid), collagen, chitosan), ceramics (e.g., bioglass, hydroxyapatite (HAP), calcium phosphate) and metals (e.g., titanium, Mg, Fe), have been explored and have great impact on tissue regeneration [5]. Several polymers have been investigated regarding their application for bone tissue regeneration. However their poor mechanical strength limits their applicability. Each material have it advantages and disadvantages, therefore, the development of multicomponent polymeric scaffold is an effective alternative to meet the requirements necessary for bone tissue engineering, and also there are several interfacial bonding mechanisms (interface phase introduction, surface modification and *in situ* growth) that can be used to improve the compatibility between the polymeric matrix and the other components (polymer, ceramic and metal) [6-9].

Polyhydroxyalkanoates (PHA), due to their low immunogenicity, nontoxicity, biocompatibility, biodegradability and mechanical properties [10] are useful for biomedical application [11]. The first PHA identified and well characterised was PHB; however, this polymer is brittleness, hardness and crystalline, which limit its application. The PHB copolymer poly-3-hydroxybutyrate-co-3-hydroxyvalerate (PHB-HV) is commonly utilised because it is less crystalline and more flexible than PHB [12]. So, the addition of valerate leads to the production of the PHB-HV with changed physicomechanical properties that enable PHB-HV manipulation to obtain the appropriate characteristics for bone substitutes.

Human adipose stem cells (hASCs) are a valuable cellular source for cell therapy [13]. hASCs are a disposable byproduct of lipoaspirates [13,14] and can differentiate into osteoblasts in a controlled manner [14]. They actively participate in tissue regeneration by secreting soluble inflammatory cytokines and trophic factors [15]. Thus, hASCs have emerged as an attractive component for bone regeneration improvement.

While hASCs have become established in a clinical setting, issues remain regarding standard cell expansion techniques that use the fetal bovine serum (FBS). Human tissue engineering cannot use animal serum due to safety concerns, such as immune reactions [16] and the risk of transmitting infectious diseases. Several studies have been conducted to replace FBS with human supplements [17-19].

Recently, our group developed a PHB-HV scaffold using a freeze-drying technique with a structure that favours hASCs colonisation, and we also substituted FBS with pooled allogeneic human serum (aHS) for a hASCs culture which promoted an osteogenic phenotype of these cells cultured in PHB-HV *in vitro* [20]. Moreover, we showed that aHS medium maintained phenotypic, functional and genetic stability of the cells and supported safe and effective transplantation [21]. Therefore, the objective of this study was to evaluate the therapeutic effects of hASCs cultured in aHS combined with PHB-HV scaffolds to promote bone regeneration synergistically with a graft vascularisation in a nude mouse model of the critical-sized calvarial defect.

2. Materials and methods

2.1. Preparation and characterisation of PHB-HV scaffolds

PHB-HV scaffolds were prepared and characterised previously [20]. PHB-HV polymer (molecular weight 425.7 kDa) provided by PHB Industrial (Serrana, Brazil) was processed to produce the scaffolds by freeze-drying technique. Briefly, PHB-HV polymer was dissolved in chloroform at 60 °C under agitation obtaining a solution 7.5% PHB-HV (m/v). The acetic acid (water phase) was added to the homogeneous polymer solution to make an emulsion. Then, this emulsion was frozen at −80 °C and freeze-dried (Telstar) for 94h to remove the solvent and water phase completely, and subsequently, the PHB-HV scaffolds were obtained. The addition of acetic acid (water phase) created two immiscible phases, where the continuous phase contained the polymer-rich solvent and the dispersed phase was water. With this approach, it was possible to have better control over porosity and pore size than just freeze-drying the polymer solution [22,23].

The scaffolds were already characterised by scanning electron microscopy (SEM; DSM950 Zeiss) and by micro-computed tomography (μ-CT; Skyscan 1072). The mechanical properties of the scaffold were also analysed in both transverse and radial directions under compression loading using a cross-head speed of 2 mm min^{-1} with a universal tensile testing machine (Instron 4505 Universal Machine) [20].

For critical-sized calvarial defects regeneration assay, the scaffolds were customised into 1 mm thick disks with a 4 mm diameter and sterilised with 15 kGy gamma radiation for 30 min.

2.2. Pooled allogeneic human serum (aHS)

The aHS was obtained from volunteers donors, who gave informed written consent according to what is approved by the Ethics Committee of the Federal University of Minas Gerais advisory board of the National Health Council (number ETIC 11668613.7.0000.5149). Different blood-group types were processed to produce batches of aHS, as previously established by our group [20].

2.3. Isolation and culture of hASCs

hASCs were isolated from lipoaspirates from 20 to 40-year-old healthy patients. The patients gave informed written consent according to the approval for this study by the Ethics Committee of the Federal University of Minas Gerais (number ETIC 11668613.7.0000.5149) advisory board of the National Health Council. The isolation and culture of hASCs were performed as previously described [20]. Briefly, the stromal vascular fraction was isolated from lipoaspirates enzymatically digested with collagenase type I (Thermo Fischer Scientific), and cultured in the basal medium at 37 °C in a humidified 5% CO_2 atmosphere. The basal medium consisted of Dulbecco's Modified Eagle's Medium-high glucose (Sigma-Aldrich) supplemented with 5 mM sodium bicarbonate, penicillin (100 units/mL), streptomycin (0.1 mg/mL), amphotericin B (0.25 μg/mL), gentamicin (60 mg/L) and 10% aHS. After approximately 28 h incubation, non-adherent cells were removed, and the hASCs maintained at subconfluent levels with three weekly medium changes. Cells at the third passage were used for all experiments.

2.4. Flow cytometry

hASCs were incubated with each primary mouse monoclonal antibody CD166, CD90, CD73-PE, CD105, CD34, CD45, HLA-DR and CD19. The cells were washed twice with PBS and then incubated with a secondary antibody. Finally, the cells were fixed with 1% paraformaldehyde. The secondary antibody was Alexa Fluor 488 goat anti-mouse

IgG. The hASCs were analysed by flow cytometry with a FACSCalibur (BD Immunocytometry Systems) using the CELLQuest acquisition software. A minimum of 15,000 events was acquired, and cell marker expression analysed with FlowJo 7.5.6 software (Treestar, Inc).

2.5. hASCs differentiation assay (multilineage potential of hASCs)

The differentiation multilineage potential of hASCs cultivated in monolayer *in vitro* was evaluated through incubation with the osteogenic, adipogenic and chondrogenic medium. Osteogenic differentiation was induced by culturing cells in an osteogenic medium that consisted of basal medium with 50 μg/mL ascorbate-2-phosphate, 10 mM β-glycerophosphate and 0.1 μM dexamethasone. Then, the differentiation was assessed by von Kossa staining. For adipogenic differentiation, cells were cultured in an adipogenic medium that consisted of basal medium with 0.5 mM isobutylmethyl-xanthine, 200 μM indomethacin, 1 μM dexamethasone, and 10 μM insulin. Oil Red O staining (Thermo Scientific) was performed following the manufacturer's instructions to indicate intracellular lipid accumulation. Chondrogenic differentiation was induced by culturing hASCs in a three-dimensional pellet in a chondrogenic medium that consisted of basal medium with 1 mM dexamethasone, 125 μg/mL bovine serum albumin, 1 mM pyruvate, 200 U/mL insulin, 3.25 μg/ml transferrin, 0.01 μg/mL transforming growth factor-β1 and 5 mg/mL ascorbate-2-phosphate with only 1% aHS. Differentiation was assessed staining with 1% Alcian Blue 8GX. hASCs were induced towards osteogenic, adipogenic or chondrogenic lineages for three weeks [14].

2.6. PHB-HV + hASCs construct

5×10^5 hASCs were seeded on the PHB-HV scaffold to prepare PHB-HV constructs (PHB-HV + hASCs). Subsequently, constructs were maintained in basal medium for five days before *in vivo* implantation.

Before implantation, cell adhesion and viability of hASCs in PHB-HV scaffolds were evaluated by SEM (DSM950 Zeiss) [20], and Calcein-AM staining. Briefly, the constructs were washed with PBS and incubated with 3 μg/mL Calcein-AM (Thermo Fischer Scientific) for 30 min, at room temperature and protected from light. The Calcein-AM-stained constructs were washed with PBS and fixed with 10% formaldehyde for 30 min. After fixation, the cells were stained with 1 μg/mL Hoechst 33258 pentahydrate (Invitrogen) for 20 min to stain the nuclei. The stained constructs were visualised using confocal microscopy (LSM 510 Meta Zeiss).

2.7. Calvaria critical sized-defect procedure

Eight-week-old male *nu/nu* athymic, Balb/c nude mice (*Mus musculus*), weighing 20 g, were used for calvaria critical sized-defect assay. This experiment was performed in accordance with the Ethical Principles of Animal Experimentation and approved by the Animal Committee of the Federal University of Minas Gerais (CEUA/UFMG protocol number 373/2012).

Thirty-six adult male Balb/c nude mice were weighed and anaesthetised with an intraperitoneal injection of 90 mg/kg ketamine and 15 mg/kg xylazine. The surgical site was cleaned with a 70% ethanol and 10% povidone-iodine solution, and an incision was made just off the sagittal midline to expose the parietal bone. The pericranium was removed, and a non-healing full-thickness 4-mm diameter defect was made in the parietal bone using a drill (Aesculap Hilan) with a brass trephine bit under constant saline irrigation. The animals were assigned to the following groups (n = 6 mice per group and time point): empty defect (control), scaffold alone (PHB-HV) and PHB-HV scaffolds loaded with hASCs (PHB-HV + hASCs). After osteotomy, the specific treatment (empty, PHB-HV or PHB-HV + hASCs) was placed into the defect, and the skin sutured with 4.0 nylon suture. None subject has the dura mater damaged. The animals were monitored during the entire experiment.

The animals have euthanised 4 or 12 weeks post-surgery, the dissected skulls photographed, and the calvaria was retrieved and immediately processed for micro-computed tomography (μ-CT), histological and immunohistochemistry analyses and real-time quantitative PCR (qPCR) analysis.

2.8. μ-CT

New bone formation was also assessed using a μ-CT system (SkyScan 1172). The analysis was performed with a high-resolution mode of 8.9 μm and an exposure time of 590 m s. The energy parameters were 48 kV and 204 μA. A threshold of 79-255 was chosen and constantly maintained for all of the scanned specimens. The segmented images obtained were three-dimensionally reconstructed using NRecon.

2.9. Real-time quantitative polymerase chain reaction (qPCR)

qPCR was performed to evaluate mouse mRNA levels of the following markers: runt-related transcription factor 2 (*RUNX2*), collagen type I alpha 1 chain (*COL1A1*), alkaline phosphatase (*ALPL*), bone gamma-carboxyglutamate protein (*BGLAP*) and vascular endothelial growth factor A (*VEGFA*). Beta actin (*ACTB*) was the reference gene and the analysis restricted to the area of the bone defect. The dissected calvaria implants were frozen in liquid nitrogen and total RNA extracted using TRIZOL reagent (Invitrogen) according to the manufacturer's protocol. RNA samples were treated with DNase (Promega), following the manufacturer's recommendation, and cDNA was synthesised with the RevertAid H Minus M-MuLV RT kit (Fermentas). The sequences of the forward and reverse primers used for amplification of *ACTB* (GenBank: NM_007393.5), *RUNX2* (GenBank: NM_001146038.2), *COL1A1* (GenBank: NM_007742.3), *ALPL* (GenBank: X13409.1), *BGLAP* (GenBank: NM_007541.3) and *VEGFA* (GenBank: NM_001287056.1) were: 5′- GGATGCAGAAGGAGATTACTG-3′ (ACTB-F′), 5′-CGATCCAG AGAGAGAGTACTTG-3′ (ACTB-R′); 5′-AATGCCTCCGCTGTTATGA AAA-3′ (RUNX2-F′), 5′-TCCGGCCCACAAATCTCA-3′ (RUNX2-R′); 5′-CTTCACCTACAGCACCCTTGTG-3′ (COL1A1-F′), 5′-TGACTGTCTTG CCCCAAGTTC-3′ (COL1A1-R′); 5′-CAGTAACCGCTGCCCGAAT-3′ (ALPL-F′), 5′-TCCTCGCCCGTGTTGTG-3′ (ALPL-R′); 5′-TGACCTCACAG ATGCCAAGC-3′ (BGLAP-F′), 5′-GCCGGAGTCTGTTCACTACC-3′ (BGLAP-R′); 5′-GTACCTCCACCATGCCAAGTG-3′ (VEGFA-F′), 5′-TGGG ACTTCTGCTCTCCTTCTG-3′ (VEGFA-R′). qPCR reaction was carried out using 2x SYBR Green PCR Master Mix (Applied Biosystems) in a 7500 Fast Real-Time PCR System (Applied Biosystems) according to optimised methodology [21]. Data were processed using 7500 Software, version 2.3 (Applied Biosystems). Gene expression calculation was performed using the $2^{-\Delta\Delta Ct}$ method, where ΔΔCt = ΔCt (sample) - ΔCt (calibrator) and ΔCt = Ct (target gene) - Ct (reference gene). *ACTB* was used for data normalisation (reference gene), and internal control (mature bone) as a calibrator.

2.10. Histology and immunohistochemistry

For histological examination, calvaria were collected at the established endpoints, fixed in 4% paraformaldehyde for 48 h and decalcified at 4 °C for seven days with a 10% ethylenediaminetetraacetic acid solution (pH 7.2). After decalcification, the calvaria were paraffin-embedded, sectioned at 5 μm and stained with H&E.

To address the commitment of the implants with osteogenesis, we performed immunohistochemistry to detect the expression of osteocalcin, an osteoblast marker that is encoded by *BGLAP*. For immunohistochemical analysis, the cross-sections of each implant were blocked with PBS that contained 10% normal goat serum and 0.1% Tween 20 for 1 h at room temperature, and after with anti-osteocalcin antibody (1:200) for 2 h at room temperature. The slides were incubated with biotinylated anti-mouse secondary antibody (1:200) with conjugated streptavidin (1:400). Successive sections were analysed, and

representative images acquired with an optical microscope (Olympus BX-41 with a Q-Color3 digital camera; Olympus, Japan).

2.11. RT-PCR

The presence of hASCs in the area of the implants of the PHB-HV + hASCs group after 12 weeks post-implantation was assessed according to gene expression of the endothelial marker *VEGFA*. In order to do that, the RNA extracted from the dissected calvaria implants was reverse transcripted into cDNA. mRNA was also isolated from hASCs culture as a positive control. RT-PCR was performed for human *VEGFA* (GenBank: NM_001171623.1) 5′-GGAGGGCAGAATCATCACGAAG-3' (hVEGFA-F′), 5′-GGATGGCTTGAAGATGTACTCG-3' (hVEGFA-R′); amplicon size: 132 bp and mouse *VEGFA* (GenBank: NM_001287056.1) 5′-GTACCTCCACCATGCCAAGTG-3′ (mVEGFA-F′), 5′-TGGGACTTCTG CTCTCCTTCTG-3′ (mVEGFA-R′), amplicon size: 63 bp. PCR cycles were as follows: 95 °C for 3 min, 95 °C for 40 s, 60 °C for 30 s and 72 °C for 30 s (35 cycles), and 72 °C for 5 min. A non-template control (NTC) was performed for each pair of primer evaluated. The RT-PCR products were analysed through 2.5% agarose gel electrophoresis and visualised with ethidium bromide and 50 bp DNA step ladder (Sigma).

2.12. Quantification of vessel density

The number of vessels was quantified in consecutive fields of five non-consecutive H&E-stained tissue sections at the fixed endpoints and group using ImageJ software (NIH). The result represents the mean number of vessels/mm^2 for each group.

2.13. Statistical analyses

Statistical analyses were performed using Graph Pad Prism 5.0. The values represent the mean ± standard error of the mean. New bone formation assessed by μ-CT was analysed using one-way, and two-way ANOVA followed by Bonferroni's post-test. Data on vessel density were analysed using a one-way ANOVA and Bonferroni's post-test, and qPCR data were analysed using two-way ANOVA and Bonferroni's post-test. Significant differences between the groups, determined using post-tests, were set with $p < 0.05$.

3. Results

3.1. Scaffold characteristics

The scaffolds show porosity of 88.1%-0.3% and an anisotropic and highly interconnected porous structure with an average pore size of 163.5 ± 0.1 μm as revealed by μ-CT analysis Fig. 1. Moreover, the scaffolds present better mechanical properties in the transverse direction (32.09-0.273 MPa) than in the radial direction (1.24-0.307 MPa) [20].

3.2. hASCs

hASCs depicted mesenchymal nature. Plastic-adherent isolated hASCs had a fusiform morphology Fig. 2a. The mesenchymal phenotype of the isolated population was confirmed by their multipotency Fig. 2b. The hASCs differentiated into osteogenic, adipogenic and chondrogenic lineages, as demonstrated by staining of mineralised matrix deposits, intracellular lipid vacuoles and glycosaminoglycan, respectively. The hASC immunophenotype was consistent with mesenchymal stem cells (MSC). More than 90% of the cells expressed CD105, CD166, CD90 and CD73. Cells were negative for the hematopoietic markers CD34, CD45, CD19 and HLA-DR Fig. 2c.

3.3. PHB-HV + hASCs construct

hASC viability was preserved after being seeded on PHB-HV scaffolds. SEM micrographs showed a highly porous structure with high cell density in the inner scaffold region after five days of culture Fig. 3a. Immediately before implantation, cells were still viable and distributed throughout the scaffold, as indicated by calcein-AM staining Fig. 3b.

3.4. Defect healing by hASCs loaded on PHB-HV scaffolds in nude mice

No evidence of infection or scaffold extravasation occurred post-operatively or upon harvesting the calvarial implants. Bone healing was assessed macroscopically. After 4 or 12 weeks, the bone defect was apparent in the control group; there was a lack of healing, and the brain, meninges and meningeal vessels were apparent. In both scaffold groups, the scaffold was visible at the site of implantation and integrated with the adjacent tissue Fig. 4a.

Bone healing progression analysis was performed using H&E staining Fig. 4b. The implanted PHB-HV scaffolds were integrated into the adjacent bone and not biodegraded after 12 weeks. Neither the implants nor adjacent tissue was necrotic. Twelve weeks after implantation, no animal of any group had complete bone defect healing. The control group exhibited no bony regeneration. Nevertheless, the PHB-HV group showed some ossification that produced small mineralised bone matrix (primary bone) that was not contiguous with the bony front. Besides, new bone formation localised in the areas of the scaffold adjacent to the dura mater or periosteum within the defect.

In general, 4 weeks post-implantation, the PHB-HV- and PHB-HV + hASCs-implanted animals displayed a mild multifocal lymphohistiocytic inflammatory infiltrate associated with giant cells and amorphous material (e.g., the PHB-HV scaffold). The PHB-HV scaffold triggered a foreign body reaction that increased between 4 and 12 weeks post-surgery, while the bone defect in the control group was

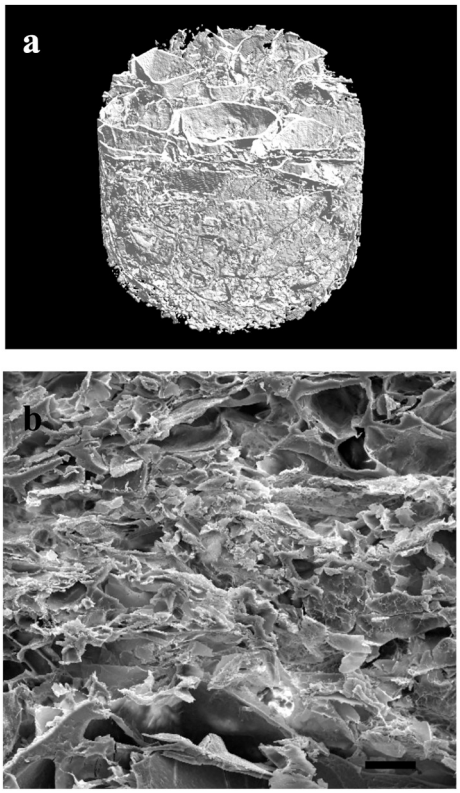

Fig. 1. PHB-HV scaffold characterisation. a. Three-dimensional μ-CT of PHB-HV scaffold. b. Representative micrograph of the internal structure of the scaffolds. Scale bar is 50 μm.

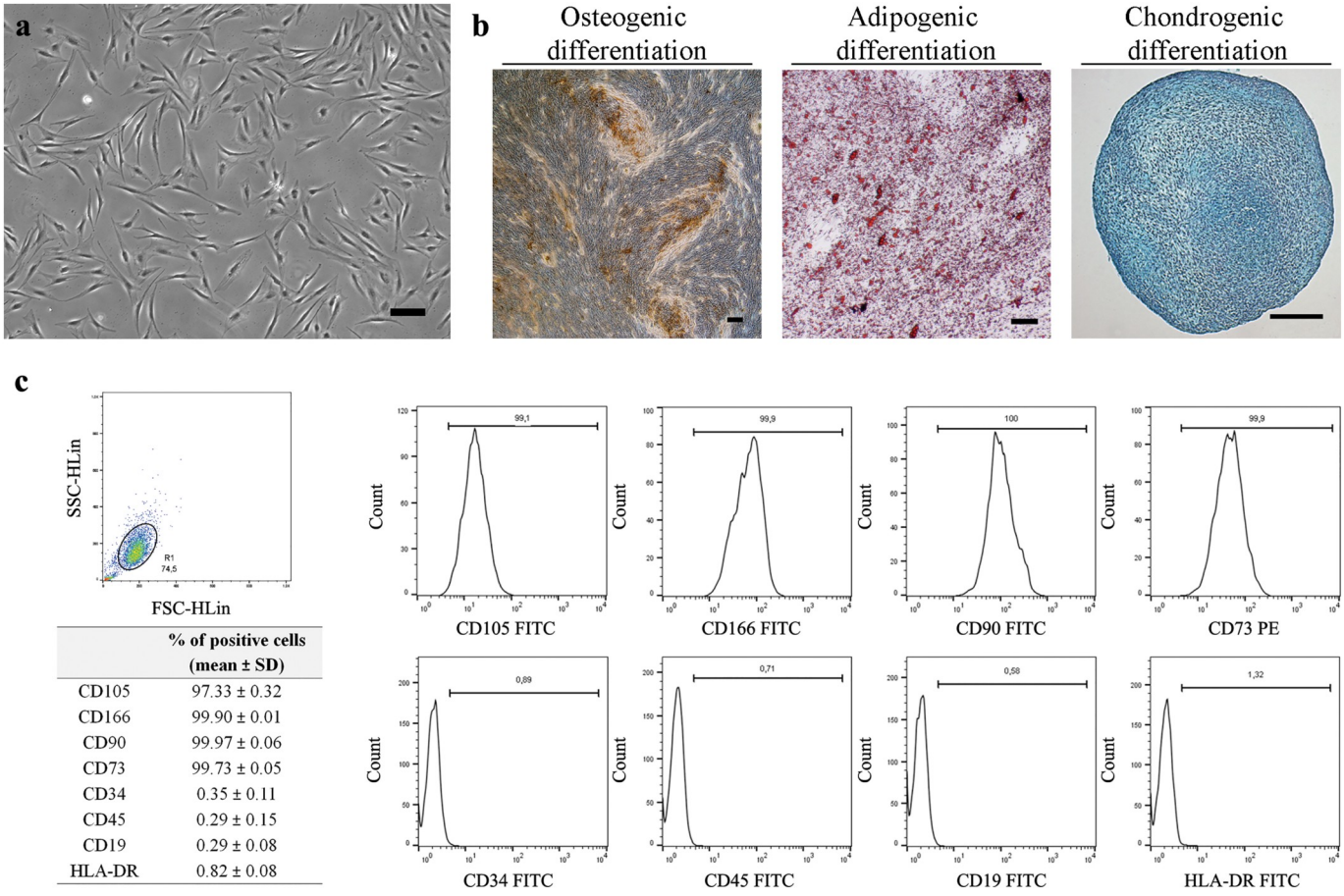

	% of positive cells (mean ± SD)
CD105	97.33 ± 0.32
CD166	99.90 ± 0.01
CD90	99.97 ± 0.06
CD73	99.73 ± 0.05
CD34	0.35 ± 0.11
CD45	0.29 ± 0.15
CD19	0.29 ± 0.08
HLA-DR	0.82 ± 0.08

Fig. 2. Characterisation of human adipose tissue stem cells cultured in basal medium supplemented with aHS. a. Fusiform morphology of hASCs; scale bar is 150 µm. b. hASCs capacity to differentiate into the osteogenic, adipogenic and chondrogenic lineages, respectively, shown by the staining of mineral deposits in the extracellular matrix with von Kossa, lipid vacuoles with Oil Red O and glycosaminoglycan with Alcian blue; scale bar is 150 µm. c. Representative histograms depicted mesenchymal phenotype characterised by the expression of selected mesenchymal stem cell markers. The cell population expressed CD105, CD166, CD90 and CD73, but did not express CD34, CD45, CD19 and HLA-DR. (For interpretation of the references to colour in this figure legend, the reader is referred to the Web version of this article.)

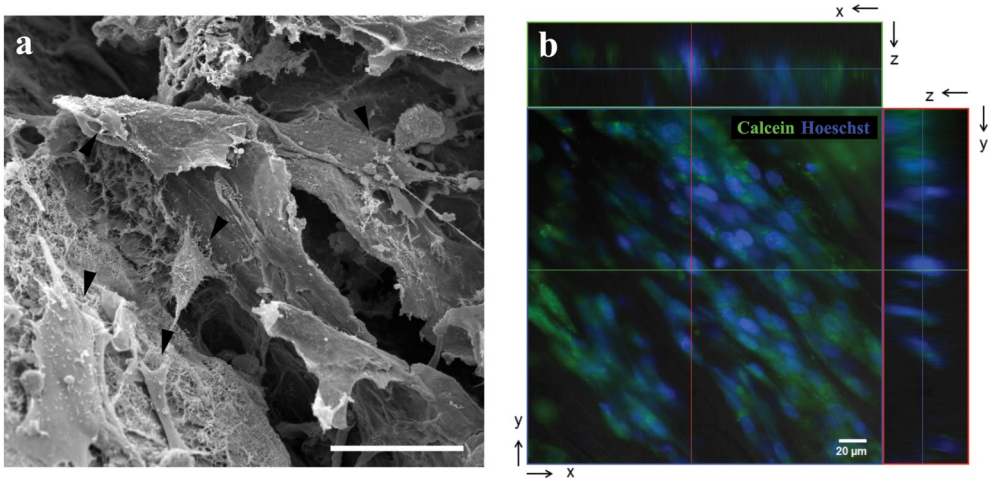

Fig. 3. hASCs adhered to the PHB-HV scaffold. a. Scanning electron micrograph of the inner region of the PHB-HV scaffold showed hASCs adhered. Black arrowhead indicates cells; scale bar is 50 µm. b. The x-y cross-section shows Calcein-AM staining (green signal), indicative of viable hASCs adhered to the PHB-HV scaffold, immediately before transplantation. An orthogonal projection of two cross-section cuts (x-z and y-z) is also shown. Nuclei were in blue. Scale bar is 20 µm. (For interpretation of the references to colour in this figure legend, the reader is referred to the Web version of this article.)

substituted by elongated cells with minimal lymphohistiocytic inflammatory infiltrate. Twelve weeks post-implantation, the PHB-HV and PHB-HV + hASCs groups showed fibrous connective tissue interspersed with the scaffolds. For the PHB-HV group, primary bone appeared as islands within the area of the bone defect. After 12 weeks, the PHB-HV + hASCs group presented a dense fibrous connective tissue in the injured area and did not display mineralised bone matrix Fig. 5.

3.5. µ-CT

µ-CT scans revealed little to no bone healing in the PHB-HV or PHB-HV + hASCs groups. Quantification of µ-CT images showed that empty defects (control) healed by less than 5% over 12 weeks. Defects treated with scaffolds (PHB-HV or PHB-HV + hASCs) healed approximately 10% after 12 weeks. Nevertheless, there was no significant difference in

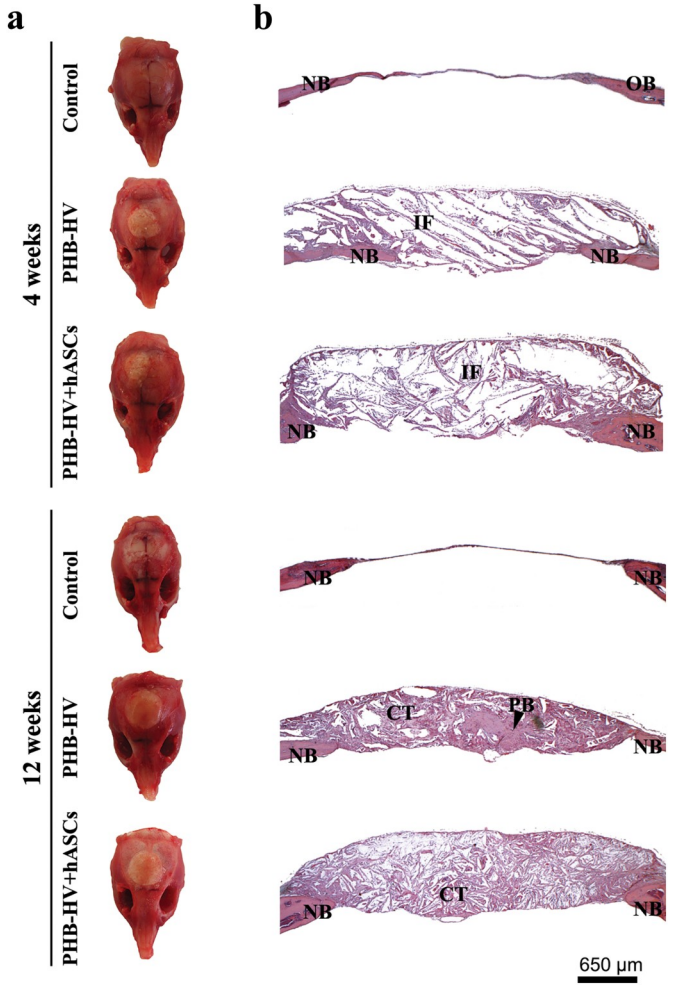

Fig. 4. Bone healing evaluation of calvarial defects from immunodeficient (nude) mice. a. Gross appearance of calvarial defects. Macroscopic images of the harvested skulls demonstrated the brain, meninges and meningeal vessels in the control group with no visible bone healing. PHB-HV and PHB-HV + hASCs groups showed the scaffold, and neither the brain nor meninges were visible. n = 6 per group. b. Representative images of H&E-stained histological sections of bone defects at 4 and 12 weeks post-implantation that highlight tissue regeneration progression over time. Islands of primary bone were observed only in the PHB-HV group 12 weeks post-implantation (black arrowhead). Abbreviations: IF, inflammatory infiltrate; NB, native bone; PB, primary bone; CT, fibrous connective tissue. Scale bar is 650 µm.

bone formation between the control and both treatment groups as well as between 4 weeks and 12 weeks for each group evaluated, Fig. 6.

3.6. Bone markers expression

The potential PHB-HV scaffold biomechanical effect on neo-tissue formation could involve extracellular matrix deposition and organisation and may enhance the ability of hASCs to regenerate bone by direct differentiation into osteogenic precursors or through soluble factors release. Almost all bone markers were significantly lower in PHB-HV and PHB-HV + hASCs groups compared to native, uninjured bone 4 and 12 weeks post-implantation. The one exception was *BGLAP* in the PHB-HV + hASCs group 12 weeks after implantation, where the expression of this gene was similar to a native bone. Further, *BGLAP* and *RUNX2* expressions were significantly higher in the PHB-HV + hASCs group at both post-implantation time points, compared to the PHB-HV group Fig. 7a-b. *COL1A1* expression was significantly higher in the PHB-HV + hASCs group compared to the PHB-HV group only at 12 weeks post-implantation Fig. 7c. *ALPL* level was similar for the PHB-HV and PHB-HV + hASCs at both time points Fig. 7d. Overall, there was a general trend for increased expression of these bone markers in the PHB-HV + hASCs group over time.

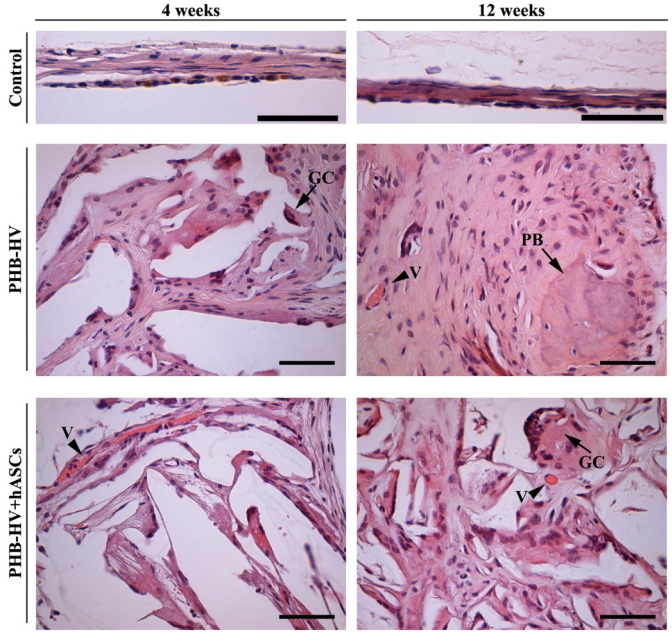

Fig. 5. High magnification representative images of H&E-stained histological sections of the inner implant region over time. Fibrous connective tissue interspersed with scaffolds and foreign body reaction was apparent for both the PHB-HV and PHB-HV + hASCs groups. Suggestive mineralised bone matrix focus was observed in the PHB-HV group after 12 weeks post-implantation. Abbreviations: GC, giant cell; V, vessel; PB, primary bone. Scale bar is 50 µm.

Immunohistochemical staining was demonstrated in both scaffold groups osteocalcin-positive cells after 4 and 12 weeks post-implantation. However, signal intensity was markedly higher for the PHB-HV + hASCs compared to the PHB-HV group 12 weeks after implantation; osteocalcin staining was apparent in cells in the matrix that comprised the connective tissue. In the control group, only the native bone expressed osteocalcin Fig. 7e.

3.7. Transplanted hASCs improved neovascularisation

Gene expression of the angiogenic factor *VEGFA* demonstrated the influence of transplanted hASCs and PHB-HV scaffold on neovascularisation. Human *VEGFA* mRNA was detected only in the PHB-HV + hASCs group after 12 weeks, not being detected in the other groups, while mouse *VEGFA* mRNA was detected in all groups evaluated by RT-PCR Fig. 8a. Mouse *VEGFA* expression was significantly higher for the PHB-HV + hASCs group compared to all other groups 4 weeks post-implantation. Comparatively, increased *VEGFA* expression was detected only 12 weeks post-implantation for the PHB-HV group Fig. 8b. Vessel density quantification confirmed this result. This analysis revealed moderate multifocal neovascularisation with a significantly higher vessel density for PHB-HV + hASCs compared to the control and PHB-HV groups 4 weeks post-implantation. The PHB-HV group achieved an equivalent number of vessels in the implant compared to the PHB-HV + hASCs group only after 12 weeks. The control group did not display significant neovascularisation Fig. 8c.

4. Discussion

Bone tissue engineering is a promising strategy to treat bone injuries, but challenges remain to obtain enough cells, to optimise culture conditions and to develop efficient structural matrices.

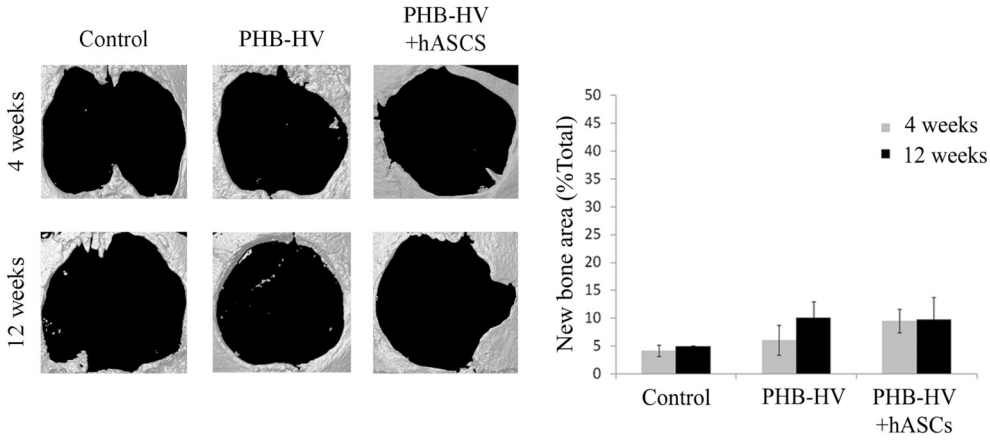

Fig. 6. μ-CT images of calvarial defects 4 and 12 weeks post-implantation. The area of newly regenerated bone in each defect was calculated for each experimental group and expressed as a percentage of the entire defect area. There was no statistical difference between the groups at each time evaluated and between the times of 4 and 12 weeks post-implantation.

Natural biodegradable polymers, such as PHB-HV, are investigated for tissue engineering applications. Among scaffold fabrication techniques, the freeze-drying technique has been useful to create high-porosity scaffolds and control the pore size. In our previous studies, the PHB-HV scaffolds developed by the conventional freeze-drying technology showed a highly interconnected porous structure and mechanical performance to support tissue engineering applications. The developed PHB-HV scaffolds showed the ability to support the *in vitro* culture of CNS-derived cells and hASCs [20,23], which unveiled the lack of a cytotoxic effect of these scaffolds and from any residual acetic acid or solvent from scaffold fabrication. Also, the histocompatibility study (subcutaneous implantation) showed that PHB-HV scaffolds were well tolerated by the host tissue with no evidence of abscess formation or tissue necrosis [23]. So, it seems that the acetic acid and solvent involved in the scaffold manufacturing had been completely removed during the freeze-drying process and any substance released from the scaffold can be considered nontoxic or were bellow the harmful concentration to the host tissue. Lastly, the PHB-HV scaffold was suitable for allowing hASCs colonisation, growth and differentiation into osteogenic phenotype in an *in vitro* condition [20], which prompted us to investigate its properties *in vivo*.

Several clinical trials over the past few years have also evaluated the applicability of hASCs for regenerative medicine [24], and a myriad of advantages substantiates the use of hASCs for bone tissue engineering: an autologous cell source; cells that can be harvested by minimally invasive procedures; rapid expansion; the ability to differentiate into multiple lineages. In this study, hASCs were isolated from lipoaspirate byproducts and displayed morphology, differentiation potential and an immunophenotype that were in accordance with the International Federation for Adipose Therapeutics and Science and International Society for Cellular Therapy.

As far as we know, this is the first study to evaluate the bone regeneration capacity of hASCs cultured in aHS and combined with PHB-HV scaffold in an athymic nude mouse model of a non-healing critical-sized calvarial defect. Before implantation, the colonisation of scaffolds by hASCs showed viable cells distributed through the inner scaffold region.

Post-implantation, complete wound closure was observed at the suture site. Histological analysis demonstrated that the PHB-HV scaffold effectively substituted the bone defect and integrated with the adjacent viable bone. A foreign body reaction response was triggered, and this could influence the material's biodegradability and tissue remodelling in the long term since multinucleated giant cells were in the tissue. Giant cells are responsible for secret pro-inflammatory cytokines, chemokines and proteolytic enzymes as well as phagocytise degraded biomaterial particles [25]. However, the scaffold did not degrade after 12 weeks of implantation, and there was limited evidence of new bone formation for the PHB-HV + hASCs group. The first evidence of primary bone formation in this study was in the PHB-HV group, next to the dura mater, after 12 weeks. Three-dimensional reconstruction of μ-CT scans also revealed small areas of new bone in PHB-HV and PHB-HV + hASCs groups with no significant difference in regenerated bone volume between the groups. Other works showed that PHB-HV degrades *in vivo* into (R)-3-hydroxybutyric acid and 3-hydroxyvaleric acid, ketone bodies that exist under normal physiological conditions in human blood [23] and that PHB-HV scaffolds degrade slower than other polymeric scaffolds being noticeable only after 16 weeks *in vivo* [26]. So we could observe a synergic action between the slow new bone formation and slow scaffold degradation. Strategies such as use a biodegradable polymer to produce a multicomponent scaffold could favour the development of scaffolds with bioactivity and biodegradability adequate to bone tissue engineering application, once it is possible to take the advantage from each of the components independently [6]. For instance, PLLA is a biocompatible and biodegradable polymer, but with poor mechanical properties and also elicits a harmful local inflammatory response. Therefore to overcome these characteristics some studies have been using this PLLA with other components, such as nano magnesium oxide (nMgO) that enhance the crystallinity of the PLLA, and also neutralize the acid degradation by-products of PLLA, avoiding local inflammation [27]; and blend of PLLA, polyetheretherketone (PEEK) and β-tricalcium phosphate (β-TCP) to fabricate scaffolds by selective laser sintering (SLS) which also showed good capacity of bone regeneration associated with good biodegradability *in vivo* [28].

Both PHB-HV and PHB-HV + hASCs constructs modulated *RUNX2, ALPL, BGLAP and COL1A1* expression; hASCs addition further augmented their expression. The expression of these bone markers mRNA before osteoblast mineralisation initiation suggests that the proteins may be involved in the preparation of the extracellular matrix for the ordered deposition of minerals which is necessary for the progressive formation of new bone tissue [29]. The higher *BGLAP* expression 12 weeks after implantation is in accordance with its expression only post-proliferatively with the onset of nodule formation. Once *BGLAP* encodes the protein osteocalcin, there was a gene and protein expression correlated, and the overexpression of osteocalcin markedly higher for the PHB-HV + hASCs compared to the PHB-HV group corroborates the *BGLAP* expression observed. The *in vitro* study also showed that hASCs cultured in PHB-HV and aHS, without any further stimulus, was able to induce hASCs to an osteogenic phenotype with the evidence of increased alkaline phosphatase activity [20], which is considered an early marker of osteogenic differentiation [30,31]. Moreover, hASCs *in vitro* were able to express the genes associated with osteogenesis: *RUNX2*, *COL1A1* and *ALPL*, but not *BGLAP* [20]. Nevertheless, the observed *in vitro* results [20], and the expression of the bone markers *in vivo* were not enough to promote a significant bone healing and, despite this, the bone regeneration achieved by PHB-HV + hASCs was inferior compared to the PHB-HV group.

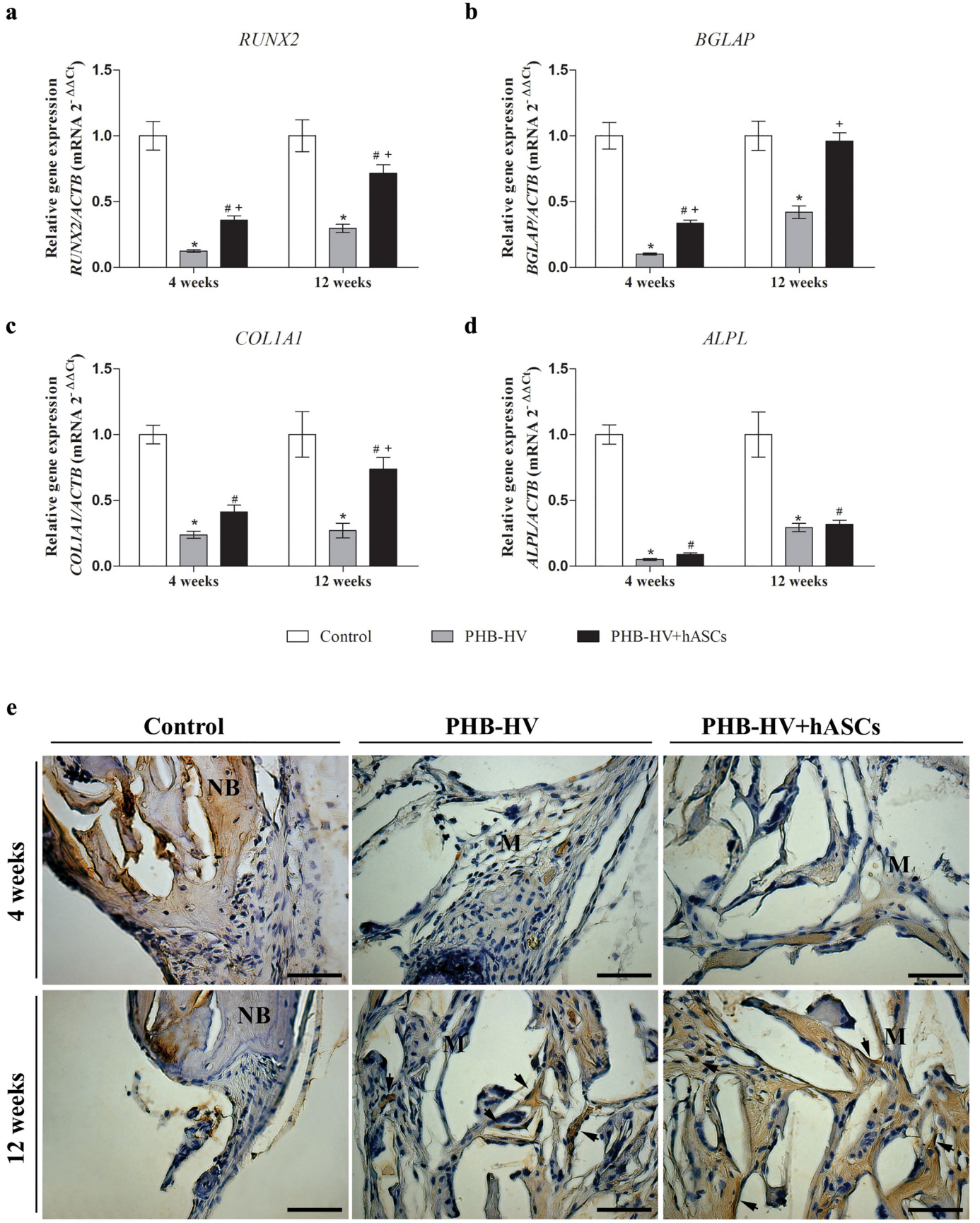

Fig. 7. Expression of bone differentiation markers. Graphs of relative gene expression of a. *RUNX2*, b. *BGLAP*, c. *COL1A1* and d. *ALPL* among the groups at 4 and 12 weeks post-implantation. $^{*}p < 0.05$, comparing PHB-HV vs control; $^{\#}p < 0.05$, comparing PHB-HV + hASCs vs control; $^{+}p < 0.05$, comparing PHB-HV vs PHB-HV + hASCs and e. osteocalcin immunohistochemical staining of implant sections at different times post-implantation. Arrow indicates cells positive for osteocalcin. Scale bar is 50 μm. Abbreviations: NB, native bone; M, matrix.

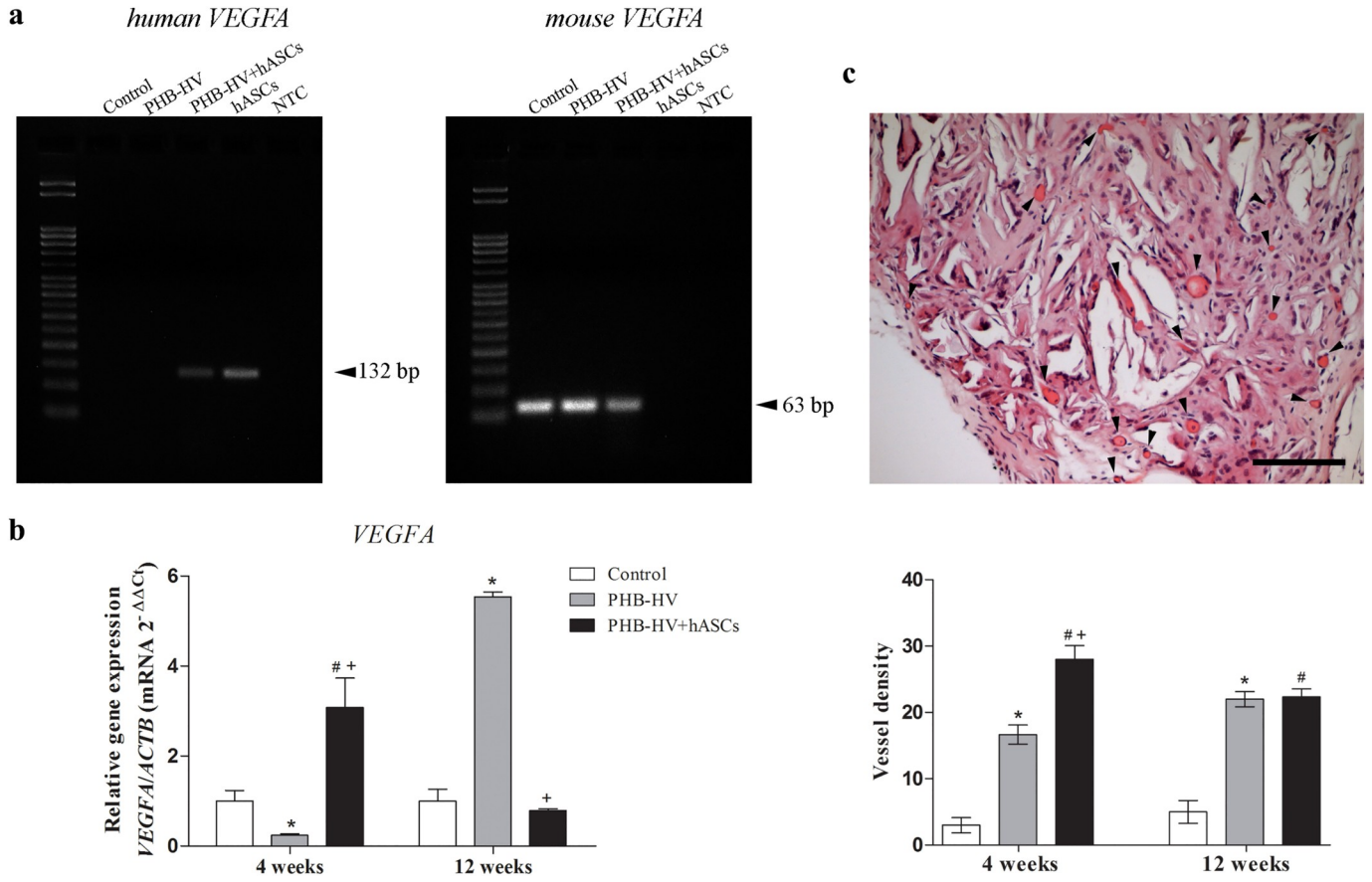

Fig. 8. Examination of the effect of PHB-HV and hASCs on neovascularisation. a. Agarose gel electrophoresis of RT-PCR analysis showing human *VEGFA* mRNA expression by PHB-HV + hASCs group and mouse *VEGFA* mRNA expression by control, PHB-HV and PHB-HV + hASCs groups 12 weeks post-implantation (50 bp DNA step ladder). b. Graphical representation of qPCR analysis of mouse *VEGFA* expression among the groups at different time points after implantation. *$p < 0.05$, comparing PHB-HV vs control; $^{\#}p < 0.05$ comparing PHB-HV + hASCs vs control; $^{+}p < 0.05$, comparing PHB-HV vs PHB-HV + hASCs. c. Representative image of the PHB-HV + hASCs group 12 weeks post-implantation that shows the blood vessels stained with H&E and graph of vessel density (mean number of vessels/mm^2) at different time points after implantation. Quantification was performed using H&E-stained sections. Black arrowheads indicate the vessels. *$p < 0.05$, comparing PHB-HV vs control; $^{\#}p < 0.05$ comparing PHB-HV + hASCs vs control; $^{+}p < 0.05$, comparing PHB-HV vs PHB-HV + hASCs. Abbreviations: hASCs, human adipose stem cells; NTC, non-template control.

The hASCs in aHS associated with PHB-HV scaffold did not promote new bone formation directly *in vivo* like expected by results of the previous *in vitro* study [20]. However, a clinically relevant finding is that hASCs survived *in vivo* even after a long period of implantation, since human *VEGFA* was detected in PHB-HV + hASCs group after 12 weeks post-implantation.

The fact that the enhanced vessel numbers were noticeably higher in the PHB-HV + hASCs group, compared to the PHB-HV group, suggests that hASCs contributed to enhancing early vascularisation. Vascularity of the scaffolds is essential and perhaps the most critical factor in graft healing because the vessels network is responsible for the diffusion of oxygen and nutrients and this blood supply supports graft viability and explains the efficacy of tissue reconstruction. The process of new blood vessel formation starts by an angiogenic signal, which can be released by tissues in response to hypoxia [32]. In response to this angiogenic signal, pericytes and endothelial cells migrate towards the angiogenic stimulus, and together with stem cells, proliferate to generate the new blood vessel. Moreover, the porosity and pore size of the scaffold can significantly affect neovascularisation and osteogenesis upon *in vivo* implantation. One of the major limitations to tissue regeneration is the relative lack of vascular supply, and much of the regenerated bone is limited in diameter due to cell diffusion limits. Combining hASCs expanded in aHS with the PHB-HV scaffold appeared to stimulate early tissue vascularisation. However, this neovascularisation did not influence bone formation. Indeed, hASCs can secrete angiogenic factors, such as VEGF, HGF and bFGF, which play essential roles during angiogenesis [33,34]. *VEGFA* is considered the most potent angiogenic factor and higher *VEGFA* expression 4 weeks post-implantation in the PHB-HV + hASCs compared to the other groups correlated with the presence of hASCs in the defect site and suggests that the transplanted cells are responsible for this upregulation and the increased number of new vessels. However, PHB-HV also induced higher *VEGFA* expression and neovascularisation at 12 weeks post-implantation that was equivalent to PHB-HV + hASC group. Possibly the PHB-HV scaffold architecture, developed by freeze-drying technique, with the pore size of 163.5 ± 0.1 μm, the porosity of 88.1% ± 0.3 and high interconnectivity, created a microenvironment which induced proper angiogenic signals (*VEGFA*) observed 12 weeks post-implantation. Besides, this microenvironment also must have allowed the cells located at the surrounding area of implantation, such as pericytes, endothelial cells, stem cells, migrated to within the scaffold and proliferated to create the vascular network at 12 weeks post-implantation. This result corroborates with other studies that showed that greater pore size (minimum recommended pore size of 100 μm) leads to increased neovascularisation of scaffolds and consequently better osteogenesis [35-37]. In addition to pore size, the higher porosity, as well as pore

interconnectivity, allow for *in vivo* bone and vessels ingrowth, being scaffolds with 80-88% of porosity ideal for vascularisation and bone tissue formation *in vivo* [38].

Other studies evaluated the capacity of hASCs for bone regeneration. However, there is a lack of consensus regarding the osteogenic potential of hASCs [39,40]. Our findings support a recent study that showed hASCs enhancing neovascularisation, but they are weak to promote bone regeneration [40]. There are some differences between our studies and others with better outcome with hASCs for bone regeneration. Firstly, we did not follow any pre-differentiation protocols [41,42] and hASCs genetically modified [29,43,44] *in vitro* before grafting as some studies did it. The athymic nude mouse model of non-healing critical-sized calvarial defect was chosen instead of using an immunocompetent animal model, because it is commonly used to evaluate bone regeneration [45,46] and it lacks T cells being well established for xenogeneic transplants, which would have contributed for long term persistence of hASCs in an *in vivo* graft and promoted earlier neovascularisation. However, the role of the immune system on osteoblasts is still unclear and should be considered the significance of the adaptative and innate immune systems on bone tissue repair. So the lack of T-cells must have contributed to delay osteoblast maturation and to prolong the proliferative phase of fracture healing as observed by other studies [47,48]. The inferior results of hASCs compared to bone marrow stem cells in the bone graft of immunocompromised mice were also observed by other works [40,49], confirming that the type of cell and donor site location of stem cells used could influence cell's differentiation potential and also the tissue healing capacity [50]. Still needs to elucidate the exact mechanism leading to the lower bone regeneration observed *in vivo*. We think that evaluating bone regeneration also in the immunocompetent model could reveal some points about the role of the immune system, apart from the biochemical strategies (growth and differentiation factors and proteins that promote bone formation, so on.). Also, the use of multicomponent scaffolds with osteoconductive materials could improve the actual strategy to achieve better results. Currently, nanoparticles such as hydroxyapatite [51-54], graphene oxide-Ag [55] and Ag [56,57], Mg [27], can be incorporated into a polymeric matrix for improving osteoconductivity, mechanical properties, antibacterial activity, degradation rate, benefiting regeneration of bone defects.

5. Conclusion

In summary, this study focused on PHB-HV scaffold associated with hASCs in xeno-free condition as a bone substitute. Despite the previous promising osteogenic potential *in vitro* of this strategy, this did not translate to *in vivo* findings. hASCs grafting even combined with PHB-HV scaffold were not sufficient for bone healing, and this should be considered before clinical application of hASCs for bone tissue engineering. However, this strategy caused long-term cell survival on the graft site, and it was successful in promoting effective *in vivo* scaffold vascularisation interesting for other fields of tissue engineering or to improve other bone tissue engineering strategies.

Declaration of competing interest

No competing interests exist.

Acknowledgements

The authors thank PHB Industrial S.A. for providing the polymer and Núcleo de Cirurgia Plástica for providing the lipoaspirates. The authors also thank Eliane G. Melo, Rogéria Serakides, Gerluza A. B. Silva, Francisco A. Cotrin, Pedro H. L. Viana, íria D. D. Santos, Eduardo H. M. Nunes and Wander L. Vasconcelos for valuable contributions to this study. This work was supported by FAPEMIG, CNPq and CAPES (Brazil).

References

[1] R. Dimitriou, E. Jones, D. McGonagle, P. V Giannoudis, Bone regeneration: current concepts and future directions, BMC Med. 9 (2011) 66, https://doi.org/10.1186/1741-7015-9-66.
[2] J. Seiler, JG; Johnson, Iliac crest autogenous bone grafting: donor site complications, J. South. Orthop. Assoc. 9 (2000) 91–97.
[3] B.D. Smith, D.a. Grande, The current state of scaffolds for musculoskeletal regenerative applications, Nat. Rev. Rheumatol. 11 (2015) 213–222, https://doi.org/10.1038/nrrheum.2015.27.
[4] R. Langer, J.P. Vacanti, Tissue engineering, Science 80 (260) (1993) 920–926, https://doi.org/10.1126/science.8493529.
[5] P. Chocholata, V. Kulda, V. Babuska, Fabrication of scaffolds for bone-tissue regeneration, Materials (Basel) 12 (2019), https://doi.org/10.3390/ma12040568.
[6] P. Feng, J. He, S. Peng, C. Gao, Z. Zhao, S. Xiong, C. Shuai, Characterizations and interfacial reinforcement mechanisms of multicomponent biopolymer based scaffold, Mater. Sci. Eng. C 100 (2019) 809–825, https://doi.org/10.1016/j.msec.2019.03.030.
[7] C. Shuai, Y. Li, G. Wang, W. Yang, S. Peng, P. Feng, Surface modification of nanodiamond: toward the dispersion of reinforced phase in poly-L-lactic acid scaffolds, Int. J. Biol. Macromol. 126 (2019) 1116–1124, https://doi.org/10.1016/j.ijbiomac.2019.01.004.
[8] A. Ashori, M. Jonoobi, N. Ayrilmis, A. Shahreki, M.A. Fashapoyeh, Preparation and characterization of polyhydroxybutyrate-co-valerate (PHBV) as green composites using nano reinforcements, Int. J. Biol. Macromol. 136 (2019) 1119–1124, https://doi.org/10.1016/j.ijbiomac.2019.06.181.
[9] M. Degli Esposti, F. Chiellini, F. Bondioli, D. Morselli, P. Fabbri, Highly porous PHB-based bioactive scaffolds for bone tissue engineering by in situ synthesis of hydroxyapatite, Mater. Sci. Eng. C 100 (2019) 286–296, https://doi.org/10.1016/j.msec.2019.03.014.
[10] N. Thadavirul, P. Pavasant, P. Supaphol, Fabrication and evaluation of polycaprolactone-poly(hydroxybutyrate) or poly(3-hydroxybutyrate-co-3-hydroxyvalerate) dual-leached porous scaffolds for bone tissue engineering applications, Macromol. Mater. Eng. 302 (2017) 1–17, https://doi.org/10.1002/mame.201600289.
[11] J. Zhang, E.I. Shishatskaya, T.G. Volova, L.F. da Silva, G.Q. Chen, Polyhydroxyalkanoates (PHA) for therapeutic applications, Mater. Sci. Eng. C 86 (2018) 144–150, https://doi.org/10.1016/j.msec.2017.12.035.
[12] Y. Wang, R. Chen, J.Y. Cai, Z. Liu, Y. Zheng, H. Wang, Q. Li, N. He, Biosynthesis and thermal properties of PHBV produced from levulinic acid by ralstonia eutropha, PLoS One 8 (2013) 4–11, https://doi.org/10.1371/journal.pone.0060318.
[13] P. Bourin, B.a. Bunnell, L. Casteilla, M. Dominici, A.J. Katz, K.L. March, H. Redl, J.P. Rubin, K. Yoshimura, J.M. Gimble, Stromal cells from the adipose tissue-derived stromal vascular fraction and culture expanded adipose tissue-derived stromal/stem cells: a joint statement of the International Federation for Adipose Therapeutics and Science (IFATS) and the International So, Cytotherapy 15 (2013) 641–648, https://doi.org/10.1016/j.jcyt.2013.02.006.
[14] P. a Zuk, M. Zhu, H. Mizuno, J. Huang, J.W. Futrell, a J. Katz, P. Benhaim, H.P. Lorenz, M.H. Hedrick, Multilineage cells from human adipose tissue: implications for cell-based therapies, Tissue Eng. 7 (2001) 211–228, https://doi.org/10.1089/107632701300062859.
[15] D.J. Prockop, "Stemness" does not explain the repair of many tissues by mesenchymal stem/multipotent stromal cells (MSCs), Clin. Pharmacol. Ther. 82 (2007) 241–243, https://doi.org/10.1038/sj.clpt.6100313.
[16] J.L. Spees, C.a. Gregory, H. Singh, H.A. Tucker, A. Peister, P.J. Lynch, S.C. Hsu, J. Smith, D.J. Prockop, Internalized antigens must be removed to prepare hypoimmunogenic mesenchymal stem cells for cell and gene therapy, Mol. Ther. 9 (2004) 747–756, https://doi.org/10.1016/j.ymthe.2004.02.012.
[17] A. Aldahmash, M. Haack-Sørensen, M. Al-Nbaheen, L. Harkness, B.M. Abdallah, M. Kassem, Human serum is as efficient as fetal bovine serum in supporting proliferation and differentiation of human multipotent stromal (mesenchymal) stem cells in vitro and in vivo, Stem Cell Rev. Rep. 7 (2011) 860–868, https://doi.org/10.1007/s12015-011-9274-2.
[18] K. Bieback, A. Hecker, A. Kocaömer, H. Lannert, K. Schallmoser, D. Strunk, H. Klüter, Human alternatives to fetal bovine serum for the expansion of mesenchymal stromal cells from bone marrow, Stem Cells 27 (2009) 2331–2341, https://doi.org/10.1002/stem.139.
[19] A. Kocaoemer, S. Kern, H. Klüter, K. Bieback, Human AB serum and thrombin-activated platelet-rich plasma are suitable alternatives to fetal calf serum for the expansion of mesenchymal stem cells from adipose tissue, Stem Cells 25 (2007) 1270–1278, https://doi.org/10.1634/stemcells.2006-0627.
[20] A.C.C. de Paula, A.A.C. Zonari, T.M.D.M. Martins, S. Novikoff, A.R.P. da Silva, V.M. Correlo, R.L. Reis, D.A. Gomes, A.M. Goes, Human serum is a suitable supplement for the osteogenic differentiation of human adipose-derived stem cells seeded on poly-3-hydroxibutyrate-Co-3-Hydroxyvalerate scaffolds, Tissue Eng. A 19 (2013) 277–289, https://doi.org/10.1089/ten.tea.2012.0189.
[21] A.C. Paula, T.M. Martins, A. Zonari, S.P. Frade, P.C. Angelo, D. a Gomes, A.M. Goes, Human adipose tissue-derived stem cells cultured in xeno-free culture condition enhance c-MYC expression increasing proliferation but bypassing spontaneous cell transformation, Stem Cell Res. Ther. 6 (2015) 76, https://doi.org/10.1186/s13287-015-0030-4.
[22] N. Sultana, M. Wang, PHBV tissue engineering scaffolds fabricated via emulsion freezing/freeze-drying : effects of processing parameters, Int. Conf. Biomed. Eng. Technol. 11 (2011) 29–34.
[23] S. Ribeiro-Samy, N.a. Silva, V.M. Correlo, J.S. Fraga, L. Pinto, A. Teixeira-Castro,

H. Leite-Almeida, A. Almeida, J.M. Gimble, N. Sousa, A.J. Salgado, R.L. Reis, Development and characterization of a PHB-HV-based 3D scaffold for a tissue engineering and cell-therapy combinatorial approach for spinal cord injury regeneration, Macromol. Biosci. 13 (2013) 1576–1592, https://doi.org/10.1002/mabi.201300178.
[24] J.M. Gimble, B. a Bunnell, F. Guilak, Human adipose-derived cells: an update on the transition to clinical translation, Regen. Med. 7 (2012) 225–235, https://doi.org/10.2217/rme.11.119.
[25] J.M. Anderson, A. Rodriguez, D.T. Chang, Foreign body reaction to biomaterials, Semin. Immunol. 20 (2008) 86–100, https://doi.org/10.1016/j.smim.2007.11.004.
[26] G. Torun Köse, H. Kenar, N. Hasirci, V. Hasirci, Macroporous poly(3-hydroxybutyrate-co-3-hydroxyvalerate) matrices for bone tissue engineering, Biomaterials 24 (2003) 1949–1958, https://doi.org/10.1016/S0142-9612(02)00613-0.
[27] C. Shuai, J. Zan, F. Qi, G. Wang, Z. Liu, Y. Yang, S. Peng, nMgO-incorporated PLLA bone scaffolds: enhanced crystallinity and neutralized acidic products, Mater. Des. 174 (2019), https://doi.org/10.1016/j.matdes.2019.107801 107801.
[28] P. Feng, P. Wu, C. Gao, Y. Yang, W. Guo, W. Yang, C. Shuai, A multimaterial scaffold with tunable properties: toward bone tissue repair, Adv. Sci. 5 (2018) 1–15, https://doi.org/10.1002/advs.201700817.
[29] J.M. Lee, E.A. Kim, G.-I. Im, Healing of tibial and calvarial bone defect using Runx-2-transfected adipose stem cells, Tissue Eng. Regen. Med. 12 (2015) 107–112, https://doi.org/10.1007/s13770-014-0070-3.
[30] N. Jaiswal, S.E. Haynesworth, a I. Caplan, S.P. Bruder, Osteogenic differentiation of purified, culture-expanded human mesenchymal stem cells in vitro, J. Cell. Biochem. 64 (1997) 295–312, https://doi.org/10.1002/(sici)1097-4644(199702)64:2<295::aid-jcb12>3.0.co;2-i.
[31] J.E. Aubin, Regulation of osteoblast formation and function, Rev. Endocr. Metab. Disord. 2 (2001) 81–94, https://doi.org/10.1023/A:1010011209064.
[32] P. Carmeliet, Angiogenesis in health and disease, Nat. Med. 9 (2003) 653–660, https://doi.org/10.1038/nm0603-653.
[33] A.I. Caplan, J.E. Dennis, Mesenchymal stem cells as trophic mediators, J. Cell. Biochem. 98 (2006) 1076–1084, https://doi.org/10.1002/jcb.20886.
[34] J. Rehman, D. Traktuev, J. Li, S. Merfeld-Clauss, C.J. Temm-Grove, J.E. Bovenkerk, C.L. Pell, B.H. Johnstone, R.V. Considine, K.L. March, Secretion of angiogenic and antiapoptotic factors by human adipose stromal cells, Circulation 109 (2004) 1292–1298, https://doi.org/10.1161/01.CIR.0000121425.42966.F1.
[35] A. Artel, H. Mehdizadeh, Y.C. Chiu, E.M. Brey, A. Cinar, An agent-based model for the investigation of neovascularization within porous scaffolds, Tissue Eng. A 17 (2011) 2133–2141, https://doi.org/10.1089/ten.tea.2010.0571.
[36] X. Xiao, W. Wang, D. Liu, H. Zhang, P. Gao, L. Geng, Y. Yuan, J. Lu, Z. Wang, The promotion of angiogenesis induced by three-dimensional porous beta-tricalcium phosphate scaffold with different interconnection sizes via activation of PI3K/Akt pathways, Sci. Rep. 5 (2015) 1–11, https://doi.org/10.1038/srep09409.
[37] V. Karageorgiou, D. Kaplan, Porosity of 3D biomaterial scaffolds and osteogenesis, Biomaterials 26 (2005) 5474–5491, https://doi.org/10.1016/j.biomaterials.2005.02.002.
[38] T. Dutta Roy, J.L. Simon, J.L. Ricci, E.D. Rekow, V.P. Thompson, J.R. Parsons, Performance of degradable composite bone repair products made via three-dimensional fabrication techniques, J. Biomed. Mater. Res. A 66 (2003) 283–291.
[39] G. Liu, Y. Zhang, B. Liu, J. Sun, W. Li, L. Cui, Bone regeneration in a canine cranial model using allogeneic adipose derived stem cells and coral scaffold, Biomaterials 34 (2013) 2655–2664, https://doi.org/10.1016/j.biomaterials.2013.01.004.
[40] M.A. Brennan, A. Renaud, F. Guilloton, M. Mebarki, V. Trichet, L. Sensebé, F. Deschaseaux, N. Chevallier, P. Layrolle, Inferior in vivo osteogenesis and superior angiogeneis of human adipose tissue: a comparison with bone marrow-derived stromal stem cells cultured in xeno-free conditions, Stem Cells Transl. Med. 6 (2017) 2160–2172, https://doi.org/10.1002/sctm.17-0133.
[41] C. Di Bella, P. Farlie, A.J. Penington, Bone regeneration in a rabbit critical-sized skull defect using autologous adipose-derived cells, Tissue Eng. A 14 (2008) 483–490, https://doi.org/10.1089/tea.2007.0137.
[42] E. Yoon, S. Dhar, D.E. Chun, N.a. Gharibjanian, G.R.D. Evans, In vivo osteogenic potential of human adipose-derived stem cells/poly lactide-Co-glycolic acid constructs for bone regeneration in a rat critical-sized calvarial defect model, Tissue Eng. 13 (2007) 619–627, https://doi.org/10.1089/ten.2006.0102.
[43] B. Peterson, J. Zhang, R. Iglesias, M. Kabo, M. Hedrick, P. Benhaim, J.R. Lieberman, Healing of critically sized femoral defects, using genetically modified mesenchymal stem cells from human adipose tissue, Tissue Eng. 11 (2005) 120–129, https://doi.org/10.1089/ten.2005.11.120.
[44] Q. Chen, Z. Yang, S. Sun, H. Huang, X. Sun, Z. Wang, Y. Zhang, B. Zhang, Adipose-derived stem cells modified genetically in vivo promote reconstruction of bone defects, Cytotherapy 12 (2010) 831–840, https://doi.org/10.3109/14653249.2010.495980.
[45] D.M. Gupta, M.D. Kwan, B.J. Slater, D.C. Wan, M.T. Longaker, Applications of an athymic nude mouse model of nonhealing critical-sized calvarial defects, J. Craniofac. Surg. 19 (2008) 192–197, https://doi.org/10.1097/scs.0b013e31815c93b7.
[46] B. Levi, A.W. James, E.R. Nelson, D. Vistnes, B. Wu, M. Lee, A. Gupta, M.T. Longaker, Human adipose derived stromal cells heal critical size mouse calvarial defects, PLoS One 5 (2010), https://doi.org/10.1371/journal.pone.0011177.
[47] D. Nam, E. Mau, Y. Wang, D. Wright, D. Silkstone, H. Whetstone, C. Whyne, B. Alman, T-lymphocytes enable osteoblast maturation via IL-17F during the early phase of fracture repair, PLoS One 7 (2012), https://doi.org/10.1371/journal.pone.0040044.
[48] A.E. Rapp, R. Bindl, S. Recknagel, A. Erbacher, I. Müller, H. Schrezenmeier, C. Ehrnthaller, F. Gebhard, A. Ignatius, Fracture healing is delayed in immunodeficient NOD/scid-IL2RΓcnull mice, PLoS One 11 (2016) 1–12, https://doi.org/10.1371/journal.pone.0147465.
[49] F. Bothe, B. Lotz, E. Seebach, J. Fischer, E. Hesse, S. Diederichs, W. Richter, Stimulation of calvarial bone healing with human bone marrow stromal cells versus inhibition with adipose-tissue stromal cells on nanostructured β-TCP-collagen, Acta Biomater. 76 (2018) 135–145, https://doi.org/10.1016/j.actbio.2018.06.026.
[50] M.K. Reumann, C. Linnemann, R.H. Aspera-Werz, S. Arnold, M. Held, C. Seeliger, A.K. Nussler, S. Ehnert, Donor site location is critical for proliferation, stem cell capacity, and osteogenic differentiation of adipose mesenchymal stem/stromal cells: implications for bone tissue engineering, Int. J. Mol. Sci. 19 (2018), https://doi.org/10.3390/ijms19071868.
[51] P. Feng, M. Niu, C. Gao, S. Peng, C. Shuai, A novel two-step sintering for nano-hydroxyapatite scaffolds for bone tissue engineering, Sci. Rep. 4 (2014) 1–10, https://doi.org/10.1038/srep05599.
[52] M. Sadat-Shojai, M.T. Khorasani, A. Jamshidi, A new strategy for fabrication of bone scaffolds using electrospun nano-HAp/PHB fibers and protein hydrogels, Chem. Eng. J. 289 (2016) 38–47, https://doi.org/10.1016/j.cej.2015.12.079.
[53] Z. Chen, Y. Song, J. Zhang, W. Liu, J. Cui, H. Li, F. Chen, Laminated electrospun nHA/PHB-composite scaffolds mimicking bone extracellular matrix for bone tissue engineering, Mater. Sci. Eng. C 72 (2017) 341–351, https://doi.org/10.1016/j.msec.2016.11.070.
[54] J. Ramier, T. Bouderlique, O. Stoilova, N. Manolova, I. Rashkov, V. Langlois, E. Renard, P. Albanese, D. Grande, Biocomposite scaffolds based on electrospun poly(3-hydroxybutyrate) nanofibers and electrosprayed hydroxyapatite nanoparticles for bone tissue engineering applications, Mater. Sci. Eng. C 38 (2014) 161–169, https://doi.org/10.1016/j.msec.2014.01.046.
[55] C. Shuai, W. Guo, P. Wu, W. Yang, S. Hu, Y. Xia, P. Feng, A graphene oxide-Ag co-dispersing nanosystem: dual synergistic effects on antibacterial activities and mechanical properties of polymer scaffolds, Chem. Eng. J. 347 (2018) 322–333, https://doi.org/10.1016/j.cej.2018.04.092.
[56] C. Shuai, Y. Xu, P. Feng, G. Wang, S. Xiong, S. Peng, Antibacterial polymer scaffold based on mesoporous bioactive glass loaded with in situ grown silver, Chem. Eng. J. 374 (2019) 304–315, https://doi.org/10.1016/j.cej.2019.03.273.
[57] J.L. Castro-Mayorga, F. Freitas, M.A.M. Reis, M.A. Prieto, J.M. Lagaron, Biosynthesis of silver nanoparticles and polyhydroxybutyrate nanocomposites of interest in antimicrobial applications, Int. J. Biol. Macromol. 108 (2018) 426–435, https://doi.org/10.1016/j.ijbiomac.2017.12.007.